Available online at www.sciencedirect.com
ScienceDirect
Journal of Catalysis 248 (2007) 226–234
JOURNAL OF CATALYSIS
www.elsevier.com/locate/jcat

Structure–activity relations in Cs-doped heteropolyacid catalysts for biodiesel production

K. Narasimharao [a], D.R. Brown [b], A.F. Lee [a], A.D. Newman [a], P.F. Siril [b], S.J. Tavener [a], K. Wilson [a,*]

[a] *Department of Chemistry, University of York, Heslington, York, YO10 5DD, UK*
[b] *Department of Chemical & Biological Sciences, University of Huddersfield, Queensgate, Huddersfield, HD1 3HD, UK*

Received 15 November 2006; revised 22 January 2007; accepted 19 February 2007

Available online 25 April 2007

Abstract

A series of insoluble heteropolytungstate ($H_3PW_{12}O_{40}$ HPW) salts, $Cs_xH_{3-x}PW_{12}O_{40}$ ($x = 0.9$–3), were synthesized and characterized using a range of bulk and surface sensitive probes including N_2 porosimetry, powder XRD, FTIR, XPS, ^{31}P MAS NMR, and NH_3 calorimetry. Materials with Cs content in the range $x = 2.0$–2.7 were composed of dispersed crystallites with surface areas $\sim$100 $m^2\,g^{-1}$ and high Brönsted acid strengths [$\Delta H^0_{ads}(NH_3) = -150\,kJ\,mol^{-1}$], similar to the parent heteropolyacid. The number of accessible surface acid sites probed by α-pinene isomerization correlated well with those determined by NH_3 adsorption calorimetry and surface area measurements. $Cs_xH_{3-x}PW_{12}O_{40}$ were active toward the esterification of palmitic acid and transesterification of tributyrin, important steps in fatty acid and ester processing for biodiesel synthesis. Optimum performance occurs for Cs loadings of $x = 2.0$–2.3, correlating with the accessible surface acid site density. These catalysts were recoverable with no leaching of soluble HPW.

Keywords: Biodiesel; Transesterification; Triglyceride; Esterification; Fatty acids; Solid acid; Heterogeneous catalysis; Heteropolyacids; XPS

1. Introduction

The depletion of world petroleum reserves and increased environmental concerns have stimulated the search for alternative renewable fuels that are capable of fulfilling an increasing energy demand [1,2]. Biodiesel fuel (fatty acid methyl esters), synthesized from vegetable oils, has similar physical properties to petrochemical diesel and is considered the best alternative fuel candidate for use in diesel engines [3]. Biodiesel production involves the catalytic transesterification of long- and branched-chain triglycerides with alcohols to produce monoesters and glycerol. Current syntheses use homogeneous alkaline agents, such as K or Na alkoxides or hydroxides [4]; however, removal of the soluble base after reaction is a major problem, because aqueous quenching results in the formation of stable emulsions and saponification, rendering separation and purification of the methyl ester difficult. As a result, biodiesel production by these routes is still not cost-competitive with petrochemical diesel fuel [5].

Use of a solid base catalyst offers several process advantages, including the elimination of a quenching step (and associated contaminated water waste) to isolate the products and the opportunity to operate a continuous process [6]. Solid bases, including zeolites [7], alkali earth oxides [8] and hydrotalcites [9,10], have been investigated in transesterification reactions, and we recently reported tuneable solid bases (Li-doped CaO and Mg-hydrotalcites) for tributyrin transesterification [9,11].

Vegetable oils also contain significant amounts of free fatty acids (even more if used cooking oil is used), which poses significant processing problems in standard biodiesel manufacturing. Free fatty acids are saponified by homogeneous alkali catalysts, leading to a loss of catalyst and increased purification costs [12]. The simplest approach to improving the processing of such vegetable oils is to first esterify these free fatty acids to their alkyl esters using an acid catalyst. Thus, the development of solid acid catalysts for esterification pretreatments is crucial to improving the efficiency of biodiesel production [13].

* Corresponding author. Fax: +44 1904 432516.
E-mail address: kw13@york.ac.uk (K. Wilson).

0021-9517/$ – see front matter
doi:10.1016/j.jcat.2007.02.016

Although considerable literature exists on the esterification of simple aliphatic and aromatic acids by solid acid catalysts, such as zeolites and resins [14,15], there are few reports on fatty acid esterification [16,17]. Heteropolyacids (HPAs) are an interesting class of solid acid catalysts; however they are unsuitable for this chemistry in their native form, due to their high solubility in polar media. Recently we reported the synthesis of a zirconium phosphate-tethered, Keggin-like catalyst effective in the esterification of palmitic acid [18].

The ability to perform simultaneous esterification and transesterification with a single catalyst would further simplify the biodiesel manufacturing process. Although homogeneous Lewis acids based on carboxylic salts of Cd, Mn, Pb, and Zn [19] have shown promise, the only previous reports of solid catalysts capable of performing simultaneous esterification and transesterification [20] require temperatures of 250 °C.

HPAs and their salts are useful acid catalysts for diverse reactions that require strong acidity [21]. Although the acid forms are themselves useful solid catalysts, they are highly soluble in, and difficult to separate from, polar media [22]. Furthermore, the number of accessible surface acidic sites is low in apolar systems where they are insoluble, due to their inherently low surface areas ($<5\ m^2\ g^{-1}$). HPA grafting onto high-surface area porous supports is often used to enhance their dispersion and accessible acid sites [23]; indeed, we have successfully used phosphotungstic acid (HPW) supported on silica in apolar liquid phase reactions [24]. Nonetheless, the high solubility of HPAs still makes such supported variants unsuitable for catalyzing polar chemistry.

Alkali-exchanged HPAs (e.g., $Cs_xH_{1-x}PW_{12}O_{40}$) [25] exhibit dramatic increases in surface area and profound changes in solubility over the parent HPA; for example, salts with large monovalent ions, such as Cs^+, NH_4^+, and Ag^+, are insoluble in water [26]. Partial substitution of protons by Cs^+ also changes the number of available surface acid sites [27], with samples of composition $Cs_{2.5}H_{0.5}PW_{12}O_{40}$ exhibiting significantly higher activity than the parent acid in gas phase, acid-catalyzed reactions. There is some controversy in the literature regarding the structure of ion-exchanged HPAs. The most plausible theory has been advanced by Okuhara et al. [28], who suggested that the Cs salts consist of ultrafine crystallites in which $H_3PW_{12}O_{40}$, is epitaxially deposited on the surface of a core of $Cs_3PW_{12}O_{40}$.

In the present work, we synthesized a series of insoluble, high-surface area $Cs_xH_{3-x}PW_{12}O_{40}$ ($x = 1$–3) solid acids for esterification and transesterification, with a view to their application in biodiesel synthesis. Materials with Cs content in the range $x = 2.0$–2.3 offer excellent performance in both these reactions, and their optimal performance can be rationalized in terms of the density of accessible surface acid sites.

2. Experimental

2.1. Catalyst preparation

First, 12-phosphotungstic acid (Aldrich) was dried at 100 °C to remove the physically adsorbed water before use. CsCl (Aldrich 99.9%) was used as received. $Cs_xH_{3-x}PW_{12}O_{40}$ samples ($x = 1$, 2, 2.1, 2.2, 2.3, 2.4, 2.5, and 3) were prepared by dropwise addition of predetermined amounts of a 0.02 mol dm^{-3} CsCl aqueous–ethanol (50:50 volume ratio) solution to a 0.08 mol dm^{-3} ethanol solution of HPW at room temperature. A white precipitate formed, and the solutions were left to dry overnight at room temperature in a vacuum oven to evaporate the ethanol and water. Fine white powders were obtained by oven-drying the materials in air at 100 °C. No further pretreatments were applied to the materials, which were stored in air before analysis and reaction testing. Catalysts are abbreviated with reference to their Cs content (e.g., $Cs_{2.3} = Cs_{2.3}H_{0.7}PW_{12}O_{40}$). The extent of proton exchange by Cs and final composition of the salts were determined by elemental analysis (Table 1).

Table 1
Elemental composition of Cs exchanged HPW samples

Nominal Cs content per Keggin ion	Measured (wt%)		Actual Cs content per Keggin ion[a]	Surface elemental composition (wt%)[b]			
	Cs[a]	W[a]		Cs	W	O	P
$Cs_{1.0}$	3.9	73.0	$Cs_{0.9}$	1.8	72.0	25.1	1.1
$Cs_{2.0}$	7.9	70.0	$Cs_{1.9}$	5.1	69.6	24.2	1.1
$Cs_{2.1}$	8.4	69.7	$Cs_{2.0}$	6.8	65.8	26.2	1.2
$Cs_{2.2}$	8.8	69.5	$Cs_{2.1}$	5.3	69.0	24.6	1.1
$Cs_{2.3}$	9.5	69.2	$Cs_{2.3}$	6.2	68.9	23.7	1.2
$Cs_{2.4}$	9.9	69.0	$Cs_{2.4}$	6.5	67.7	24.7	1.1
$Cs_{2.5}$	11.0	68.0	$Cs_{2.7}$	7.6	66.6	24.6	1.2
$Cs_{3.0}$	12.1	67.1	$Cs_{3.0}$	10.4	66.3	22.1	1.2

[a] AAS analysis by dissolving the salts in standard NaOH solution.
[b] XPS analysis.

2.2. Catalyst characterization

Nitrogen porosimetry was performed on a Micromeritics ASAP 2010 instrument. Surface areas were calculated using the BET equation over the range $P/P_0 = 0.02$–0.2, where a linear relationship was maintained. Pore size distributions were calculated using the BJH model up to $P/P_0 = 0.6$. DRIFTS spectra were obtained using a Bruker Equinox FTIR spectrometer. Powder XRD patterns were collected on a Bruker D8 diffractometer using CuK_α radiation. The bulk chemical composition of samples was determined with a Hitachi atomic absorption spectrometer. XPS measurements were performed using a Kratos AXIS HSi instrument equipped with a charge neutralizer and AlK_α X-ray source. Spectra were recorded at normal emission using an analyzer pass energy of 20 eV and X-ray power of 225 W. A wide scan across the entire energy range (1100–0 eV) also was collected at a pass energy of 160 eV to check for impurities and also confirm complete loss of Cl after ion-exchange of the HPW samples with CsCl. Energy referencing was done using the valence band and adventitious carbon. Spectra were Shirley background-subtracted across the energy region and fitted using CasaXPS Version 2.1.9. ^{31}P MAS NMR spectra were obtained in single-pulse ("ZG") mode (3.5-ms pulses; 8-s delay between pulses) on a Bruker Avance 400 spectrometer, operating at a frequency of 161.98 MHz. NMR measurements were performed in 2.5-mm-o.d. rotors at a sam-

ple spin rate of 20 kHz. Spectra were referenced externally to sodium dihydrogen phosphate (0.0 ppm). Typically, line broadening of 10 Hz was applied when processing the spectra.

Ammonia adsorption flow calorimetry was performed using a system described previously based on a Setaram 111 differential scanning calorimeter (DSC) and an automated gas flow and switching system, combined with a mass spectrometer detector (Hiden HPR20) to sample the downstream gas flow [29,30].

In a typical experiment, the catalyst sample (5–30 mg) was activated at 150 °C under a dried helium flow at 5 ml min^{-1}. After activation, while maintaining the sample temperature at 150 °C, small (typically 1.0 ml, but ranging from 0.2 to 5.0 ml) pulses of the probe gas (1 vol% ammonia in helium) at atmospheric pressure were injected at regular intervals into the carrier gas stream from a gas sampling valve. The ammonia concentration downstream of the sample was monitored continuously by mass spectrometry. The pulse interval was chosen to ensure that the ammonia concentration in the carrier gas (including that adsorbed and then desorbed after the pulse had passed) returned, to zero to allow the DSC baseline to stabilize. The net amount of ammonia irreversibly adsorbed from each pulse was determined by comparing the MS signal with that recorded during a control experiment through a blank sample tube. The net heat released for each pulse, corresponding to irreversible adsorption of ammonia, was calculated from the DSC thermal curve. From this, the molar enthalpy of adsorption of ammonia (ΔH^0_{ads}) was obtained for each successive pulse. The ΔH^0_{ads} values were then plotted against the amount of (irreversibly) adsorbed ammonia per gram of the catalyst, to give a ΔH^0_{ads}/coverage profile for each catalyst. The final uptake of NH_3 and average ΔH^0_{ads} values were determined up to the point that the molar enthalpy of adsorption dropped numerically below 80 kJ mol^{-1}, which is frequently cited as the breakpoint between adsorption on sites of significant acid strength and those with no acid strength [31].

2.3. Reactivity

Esterification and transesterification were performed in a stirred batch reactor with samples withdrawn periodically for analysis on a Shimadzu GC17A gas chromatograph fitted with a DB1 capillary column (film thickness, 0.25 mm; i.d., 0.32 mm; length, 30 m), and AOC 20i autosampler. α-Pinene isomerization was performed on a Radleys carousel reaction station under air at 60 °C. For each reaction, 50 mg of air-exposed catalyst was added to 63 mmol of α-pinene (98%, Aldrich), with 0.1 cm^3 of tetradecane (99%, Lancaster) added as internal standard. Esterification was performed at 60 °C using 50 mg of catalyst, 0.01 mol of palmitic acid (98%, Aldrich), and 0.3036 mol (12.5 cm^3) methanol (98%, Fisher) with 2.5 mmol (0.587 cm^3) of hexyl ether (97%, Aldrich) as an internal standard. Transesterification was performed at 60 °C using 50 mg of catalyst, 0.01 mol (3 cm^3) of glyceryl tributyrate (98%, Aldrich), and 0.3036 mol (12.5 cm^3) of methanol with 2.5 mmol (0.587 cm^3) of hexyl ether as an internal standard. The catalyst samples were separated from the reaction mixture for recycling by centrifugation.

Reactions were run for 6 h with initial rates determined at conversions <30%, with reactions continued for 24 h. Catalyst selectivity and overall mass balances (closure >98%) were determined using reactant and product response factors derived from multipoint calibration curves.

Catalyst stability was verified by performing leaching tests in hot methanol, with $Cs_xH_{3-x}PW$ catalysts refluxed for 6 h in methanol, after which the solid was removed. The presence of soluble HPW species in the recovered methanol was subsequently investigated by assessing the activity of the residual solvent in both esterification and transesterification reactions.

A selection of commercial solid acid catalysts (SO_4/ZrO_2 [MEL], Nafion [Aldrich], and ZSM-5 [Zeolyst]) also were screened in both transesterification and esterification reactions for comparison with the best $Cs_xH_{3-x}PW$ catalyst. SO_4/ZrO_2 and ZSM-5 were activated at 550 °C and 500 °C, respectively, for 3 h, then stored in air before use.

3. Results and discussion

3.1. Catalyst characterization

The bulk and surface composition of the Cs-exchanged HPW samples were first verified by a combination of elemental and XPS analysis. Good agreement between nominal and observed bulk Cs content was observed across the range Cs_1–Cs_3. (Table 1). Fig. 1a shows how the surface composition varies with increasing bulk Cs content from 3.9 to 12.1 wt%. The almost linear increase in surface Cs and concomitant decrease in surface W confirms the incorporation of Cs into the HPW clusters rather than simple encapsulation of HPA particles with a Cs overlayer. The surface Cs content is slightly lower than the bulk, suggesting that the surface is Cs-depleted. This trend is also seen in Fig. 1b, which illustrates how the bulk and surface Cs/W atomic ratios of the $Cs_xH_{3-x}PW_{12}O_{40}$ salts compare with the bulk and nominal values (solid line). The bulk and theoretical values are in excellent agreement; however, there is a significant deviation between the surface and bulk Cs/W ratios at low Cs content. This deviation may be accounted for by structural models proposed for intermediate $Cs_xH_{3-x}PW_{12}O_{40}$ compositions, in which $Cs_3PW_{12}O_{40}$ core particles purportedly are coated with a surface layer of $H_3PW_{12}O_{40}$ clusters [25]. Such layers would be expected to attenuate the Cs signal; however, at higher Cs loadings with more $Cs_3PW_{12}O_{40}$ present, better agreement would be expected. Indeed, taking the inelastic escape depth for the Cs 3d photoelectron to be 0.7 nm, and the thickness of a $H_3PW_{12}O_{40}$ cluster to be about 1 nm, the bulk Cs signal would be expected to be attenuated by 75% by an external layer of Keggin clusters, consistent with our observed deviation.

Closer inspection of the Cs $3d_{5/2}$ state (Fig. 2, inset) reveals broadening of the Cs $3d_{5/2}$ peak with increasing Cs loading. Peak deconvolution confirms the presence of two distinct Cs species. The lowest-loading $Cs_{0.9}$ and $Cs_{1.9}$ samples exhibit a single peak at 724 eV characteristic of Cs^+. For higher loadings, a second high binding energy state evolves at 724.9 eV and grows rapidly for compositions above $Cs_{2.3}$, as illustrated

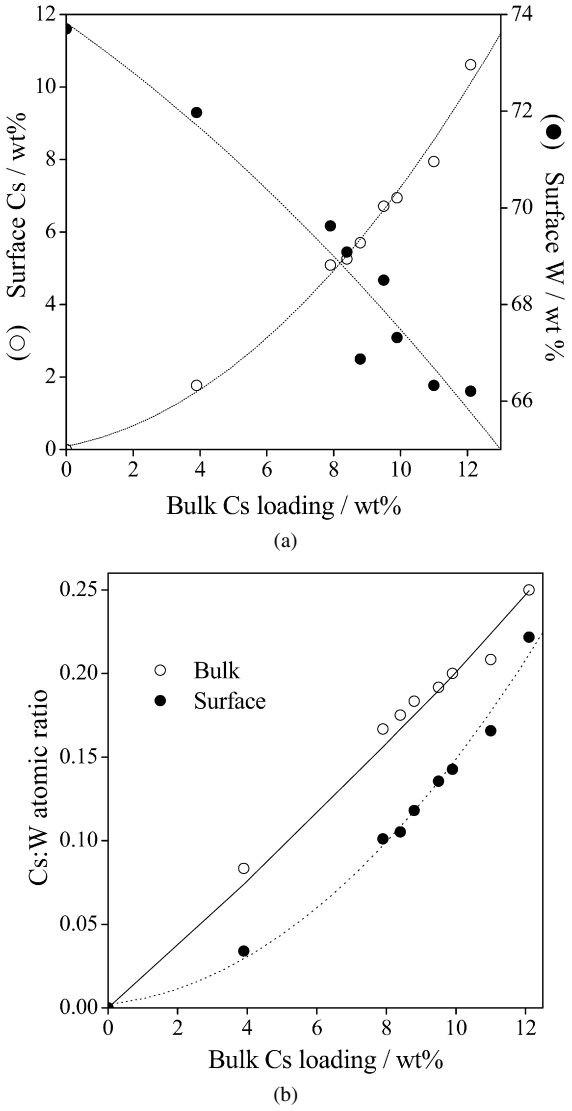

Fig. 1. (a) Surface composition of Cs exchanged HPW samples as a function of bulk Cs loading. (b) Surface and bulk Cs:W atomic ratio of Cs exchanged HPW samples as a function of bulk Cs loading.

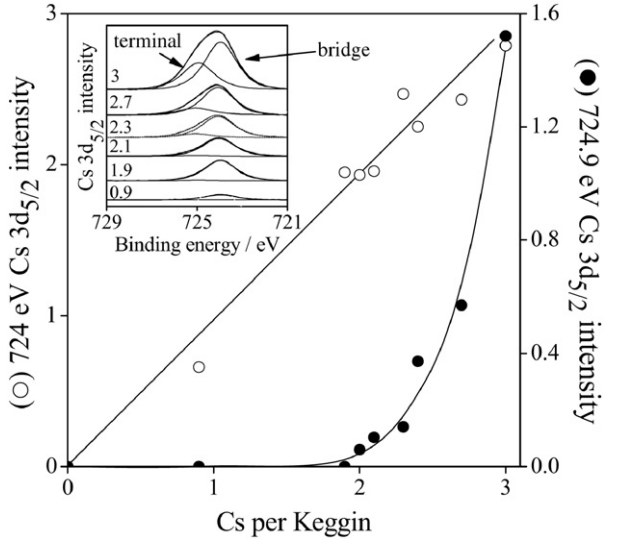

Fig. 2. Cs $3d_{5/2}$ XPS component intensity as a function of bulk Cs loading per Keggin unit in Cs exchanged HPW catalysts. Inset shows deconvoluted Cs $3d_{5/2}$ XP spectra.

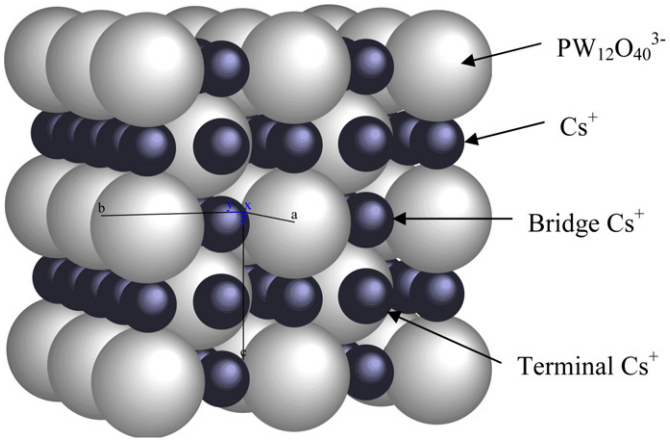

Scheme 1. Proposed structural model for $Cs_3PW_{12}O_{40}$.

in Fig. 2, where the integrated intensity of these 2 components is shown as a function of Cs per Keggin. This observation could be accounted for by the formation of a $Cs_3PW_{12}O_{40}$ core in all samples, with Cs^+ adopting a common octahedral interstitial site in the closely packed Keggin lattice, as depicted in Scheme 1. (For simplicity, only a few surface HPW units have been drawn.) Inspection of the surface-terminating layer reveals two Cs^+ coordination environments, labeled as bridge or terminal sites. Based on the relative number of these sites, we tentatively attribute the low and high binding energy components to the terminal site and bridge sites, respectively.

The powder XRD patterns of all the samples are shown in Fig. 3. $H_3PW_{12}O_{40}$ dried at 100 °C exhibits all of the reflections corresponding to a cubic *Pn3m* crystalline structure [32]. After initial doping to form $Cs_{0.9}H_{2.1}PW_{12}O_{40}$, a new set of peaks evolve as shoulders on the main HPW reflections. Diffraction peaks corresponding to the free acid disappear as the Cs content increases beyond $x = 2$. The shift in $H_3PW_{12}O_{40}$

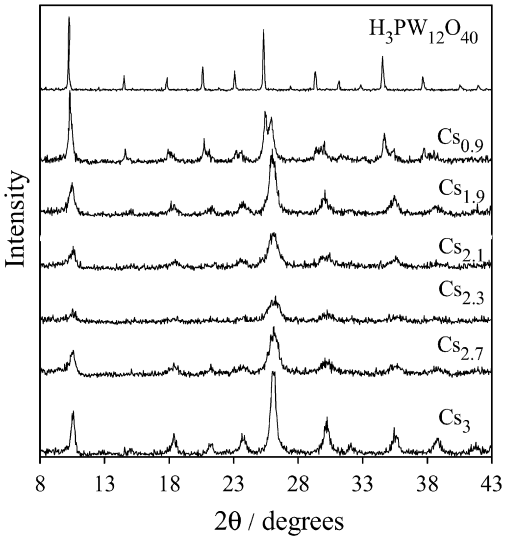

Fig. 3. Powder XRD of Cs exchanged HPW.

Table 2
Surface area, crystallite size and average pore diameters of Cs exchanged HPW samples

Catalyst	Specific surface area ($m^2\,g^{-1}$)[a]	Crystallite size (nm)[b]	Average pore diameter (nm)
H_3PW	1.0	>48.0	–
$Cs_{0.9}$	2.0	21.5	–
$Cs_{1.9}$	13.0	14.5	–
$Cs_{2.0}$	73.9	11.4	3.1
$Cs_{2.1}$	81.5	9.5	4.0
$Cs_{2.3}$	97.6	8.0	5.1
$Cs_{2.4}$	116.0	10.0	8.2
$Cs_{2.7}$	120.2	11.4	10.0
Cs_3	156.3	19.4	14.1

[a] BET equation.
[b] Estimated from XRD line width of peak ∼26°.

peaks toward higher angles in the $Cs_xH_{3-x}PW$ samples is consistent with the body-centered cubic structure of $Cs_3PW_{12}O_{40}$ salts reported in the literature [33] and indicate the presence of a unique crystalline $Cs_3PW_{12}O_{40}$ phase in all Cs-exchanged materials.

From X-ray peak broadening, it is possible to calculate the average size of the microcrystalline phases using Scherrer's equation, $D = 0.9\lambda/(\beta - \beta_0)\cos\theta$. The crystallite size ($D$ in diameter) of these Cs salts, summarized in Table 2, was calculated from this equation, where λ is the X-ray wavelength (CuK_α) in angstroms (1.54 Å), θ is the diffraction angle, β is the line width, and β_0 is the instrumental line width (0.15°, with all angles in radians). Analysis of the line widths of the XRD peaks of these Cs salts ($x = 0$–2.7) show that the size of the primary crystallites decrease from 48 to 8 nm as Cs loading increases to $Cs_{2.3}$, and particle size increases to 19.4 nm for the Cs_3 sample, indicating the formation of aggregates of the Cs_3PW core at higher Cs loadings.

The surface area of samples increase in line with these morphological changes, rising from 2 $m^2\,g^{-1}$ for $Cs_{0.9}$ to 156 $m^2\,g^{-1}$ Cs_3 observed. This is consistent with the work of Moffat et al. [34], who showed that NH_4^+ and Cs^+ salts of HPW have dense porous networks and corresponding higher surface areas than the parent HPW. Our porosimetry measurements support those findings, revealing a significant increase in the average pore diameter from 3 to 14 nm for loadings above $Cs_{2.0}$ (Table 2). Misono et al. [35] showed that large voids exist between the primary particles (microcrystallites) in these materials. If the size of the primary $Cs_{2.7}$ clusters is about 12 nm, then the most closely packed aggregates could form voids of around 3–4 nm. Interparticle voids between larger crystallites would increase the overall apparent average pore diameter, consistent with the present study.

Infrared spectra are also an informative fingerprint of the Keggin heteropoly cage structure. The Keggin anion structure consists of a PO_4 tetrahedron surrounded by 12 MO_6 (M = W, Mo) octahedra, which share edges in M_3O_{13} triads and corners with other triads through bridging oxygens. FTIR spectra of all samples, recorded after drying the samples at 100 °C, are presented in Fig. 4. These spectra exhibit similar bands for ν_{as}(P–O) = 1080 cm^{-1}, ν(W–O_c–W) = 890 cm^{-1},

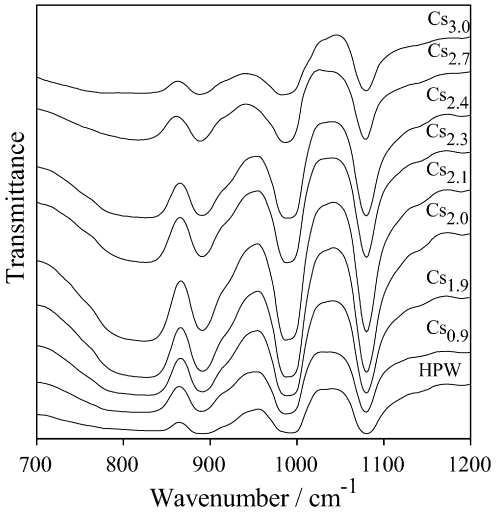

Fig. 4. DRIFT of Cs exchanged HPW.

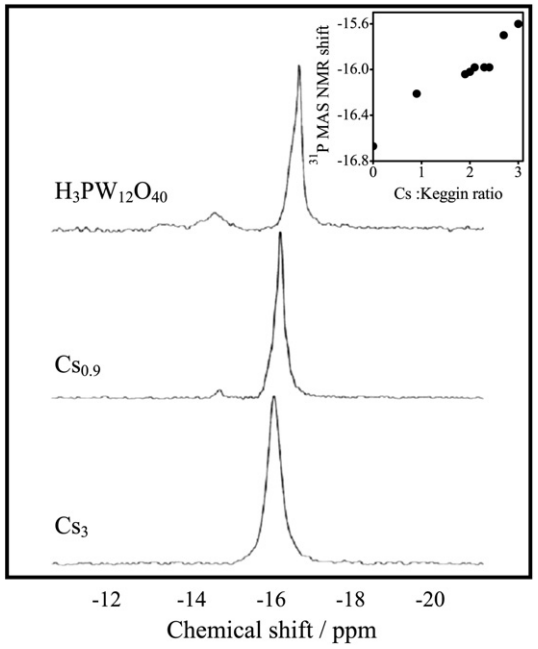

Fig. 5. ^{31}P MAS NMR of Cs exchanged HPW. Inset shows effect of Cs:Keggin ratio on chemical shift.

and ν(W–O_e–W) = 798 cm^{-1} modes. The diffuse reflectance intensity of infrared bands is known to be sensitive to particle size [36]; thus, the observed variation in the intensity of these modes may reflect a combination of the presence of smaller Keggin clusters at intermediate Cs substitutions and reduced WO_x content at the highest Cs loadings.

The ^{31}P MAS NMR spectra of HPW, Cs_1, and Cs_3 dried at 100 °C are shown in Fig. 5. Each exhibits a single peak that changes from $\delta = -16.7$ to -15.6 ppm on substitution of all 3 protons by Cs. The chemical shift dependence on Cs content per Keggin unit is presented in the inset. A small peak at -14.6 ppm was observed in the parent and Cs_1 samples, attributed to HPW with lower H_2O content. These observations are in good accord with the work of Dias et al. [37], who also found a single peak for dried $Cs_xH_{3-x}PW_{12}O_{40}$ materials but

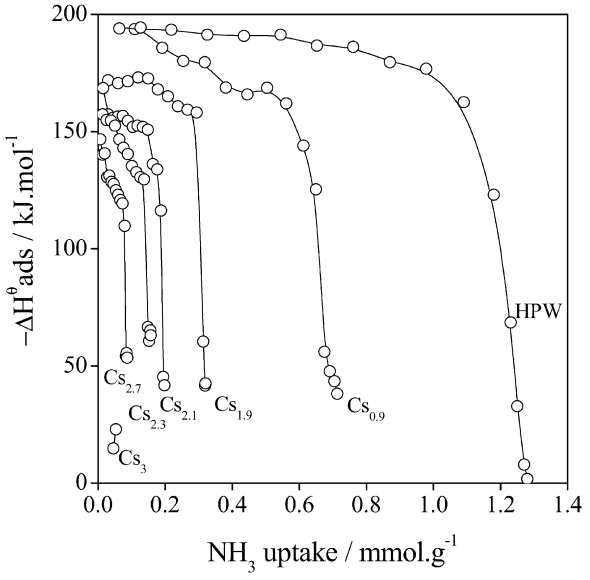

Fig. 6. NH_3 calorimetry on Cs exchanged HPW samples.

Table 3
NH_3 adsorption calorimetry data from Cs exchanged HPW samples

Sample	Average $-\Delta H^0_{ads}$ (kJ mol^{-1})	NH_3 uptake (mmol g^{-1})	Expected NH_3 uptake (mmol g^{-1})[a]
HPW	180	1.20	1.00
$Cs_{0.9}$	170	0.67	0.68
$Cs_{1.9}$	167	0.31	0.35
$Cs_{2.1}$	149	0.19	0.28
$Cs_{2.3}$	144	0.14	0.22
$Cs_{2.4}$	125	0.07	0.19
$Cs_{2.7}$	129	0.08	0.09
Cs_3	–	–	0

[a] Calculated assuming a formula $H_3PW_{12}O_{40}\cdot 6H_2O$ and a 1:1 interaction between each H^+ and NH_3, with each Cs atom replacing 2 H_2O.

multiple peaks after thermal treatment at 300 °C. The ^{31}P NMR chemical shifts correlate with the water content, because the degree of hydration decreases with Cs content in the secondary structure of the polyoxometalate.

We studied the acidity of the $Cs_xH_{3-x}PW_{12}O_{40}$ series by NH_3 flow calorimetry. Fig. 6 shows the NH_3 adsorption profiles, and Table 3 summarizes the corresponding uptakes and heats of adsorption. The incorporation of Cs lowers the number of titratable acid sites in quantitative agreement with the theoretical degree of H^+ exchange. The average heat of NH_3 adsorption falls only slightly with Cs doping up to loadings of $Cs_{2.3}$, suggesting that the residual acid strength of the Cs-doped HPW materials is not strongly perturbed during proton exchange. In contrast, however, the acidity of heavily substituted ($>Cs_{2.4}$) samples is significantly lower, in accordance with previous measurements [38].

3.2. Catalyst activity

The high solubility of HPW in polar media makes it hard to directly assess the impact of Cs doping on the catalytic performance of the parent acid during polar transformations. Consequently, we first screened the entire catalyst series against α-pinene isomerization to camphene and limonene, which is a useful apolar reaction for probing the acidity and activity of surface acid sites [24], allowing a direct comparison between pure and Cs-doped HPW samples. Table 4a presents the conversion of α-pinene and the initial rate of reaction for the series of catalysts. The table shows that catalyst activity increases with Cs content up to $x = 2.0$–2.3, then drops rapidly. By taking into account the variation in surface area and number of acid sites (determined by calorimetry), a measure of the number surface acid sites as a function of Cs:Keggin ratio can be determined, in which the total number of acid acids is weighted according to the measured surface area.

Table 4
(a) Conversion of α-pinene after 24 h reaction and initial rate of reaction observed with Cs exchanged HPW samples. (b) Conversion of palmitic acid and tributyrin observed during Cs exchanged HPW catalysed esterification and transesterification

(a)

Catalyst	Conversion of α-pinene after 24 h (%)	Initial rate of reaction (mmol$_{\alpha\text{-pinene}}$ h^{-1})
H_3PW	31	2.9
$Cs_{0.9}$	37	3.6
$Cs_{2.0}$	43	4.3
$Cs_{2.3}$	40	4.3
$Cs_{2.7}$	32	3.6
$Cs_{3.0}$	10	1.0

(b)

Catalyst	Conversion (%)		Methylbutyrate selectivity (%)[c]
	Palmitic acid[a]	Tributyrin[b]	
$Cs_{0.9}$	70.7	3.0 (10.0)	87 (85)
$Cs_{1.9}$	80.2	5.4 (14.0)	86 (86)
$Cs_{2.0}$	85.6	37.8 (65.1)	87 (87)
$Cs_{2.1}$	86.3	39.9 (68.8)	87 (88)
$Cs_{2.3}$	100.0	50.2 (82.3)	92 (95)
$Cs_{2.4}$	80.4	24.8 (44.7)	88 (89)
$Cs_{2.7}$	20.6	5.8 (17.1)	87 (87)
$Cs_{3.0}$	8.5	10.1 (15.9)	95 (96)

[a] After 6 h reaction. Selectivity to methyl palmitate >98% in all cases.
[b] After 6 h reaction, in parentheses after 24 h reaction.
[c] Glycerol formation omitted from selectivity calculation.

Fig. 7 shows a strong correlation between catalyst turnover frequency (TOF) in α-pinene isomerization and the relative number of surface acid sites. Both parameters pass through maxima around $x = 2.1$–2.3. This suggests that isomerization activity is controlled largely by the relative number of available surface acid sites, which is boosted by the higher surface areas and porosity accompanying Cs^+ exchange. Catalyst selectivity toward camphene and limonene formation was ~50 and 40%, respectively, and remained essentially independent of Cs doping across the series, consistent with their similar acid site strengths (with the exception of the Cs_3 sample, which also exhibits the lowest selectivity). These results are consistent with literature [39] reports that $Cs_{2.2}$ is more active than $Cs_{2.5}$HPAs for surface-dominated reactions, such as bistrimethylol propane monoformal hydrolysis.

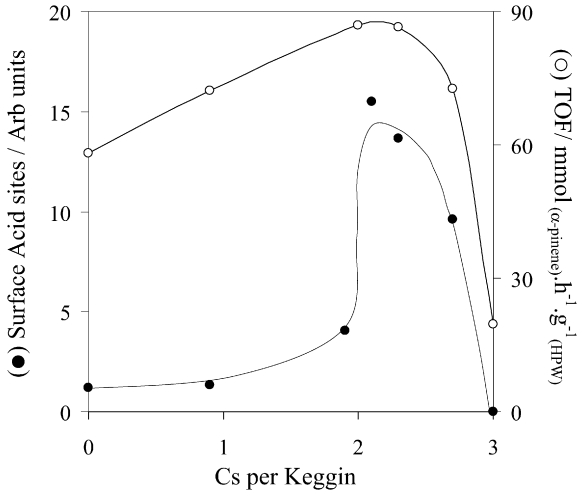

Fig. 7. Correlation between TOF in α-pinene isomerization and surface acid site density of Cs exchanged HPW catalysts.

The insoluble nature of Cs-doped HPW (with $x > 1$) in polar media makes this HPW attractive for use in esterification and transesterification reactions pertinent to biodiesel synthesis. Consequently, we evaluated the activity of Cs salts and pure HPW in the esterification of palmitic acid (a major saturated fatty acid found in palm oil) and transesterification of tributyrin (a natural constituent of butter) with methanol (Scheme 2). Fig. 8 shows the resultant palmitic acid and tributyrin conversions. The limiting conversions after 6 or 24 h of reaction are given in Table 4b. In both reactions, catalyst performance increases with Cs loading up to $Cs_{2.1}$–$Cs_{2.3}$, then decreases at higher degrees of Cs exchange.

Fig. 9 shows the time-dependent evolution of products and selectivity toward methyl butyrate for the optimal $Cs_{2.3}$ catalyst. Transesterification proceeds via progressive reaction of the triglyceride ester groups, resulting in the formation of diglyceride and monoglyceride intermediates, which are themselves ultimately converted into the methyl ester and glycerol. Although the reaction is much slower than our previous observations with hydrotalcite catalysts (24 cf. 8 h [9]), the methyl ester yield from 10 mmol of tributyrin is improved (24 mmol vs 15 mmol).

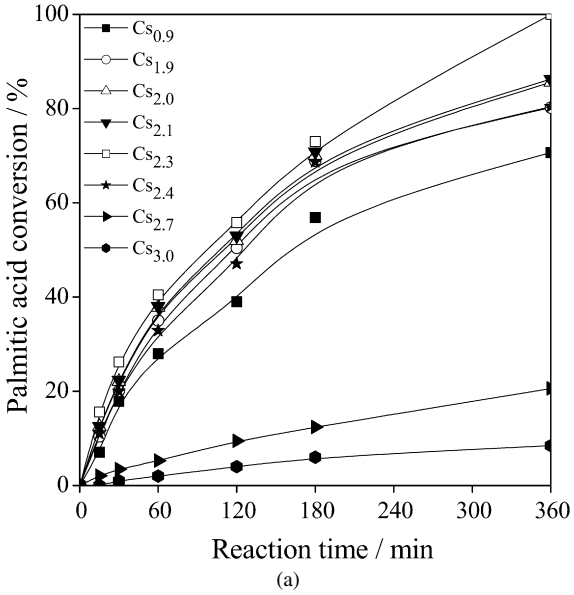

Fig. 8. (a) Conversion of palmitic acid during esterification with methanol at 60 °C using Cs exchanged HPW catalysts. (b) Conversion of tributyrin during transesterification with methanol at 60 °C using Cs exchanged HPW catalysts.

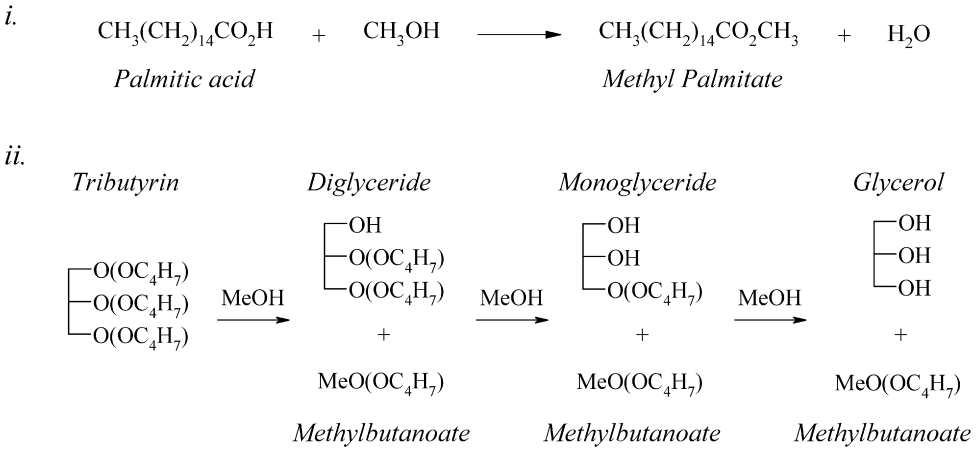

Scheme 2. (i) Esterification of palmitic acid and (ii) transesterification of tributyrin.

Table 5
Comparison of TOF and conversion for representative solid acids and bases in transesterification and esterification reactions

Catalyst	Conversion of palmitic acid (%)[a]	TOF (mmol h^{-1} g_{cat}^{-1})	Conversion of tributyrin (%)[a]	TOF (mmol h^{-1} g_{cat}^{-1})
$Cs_{2.3}$	73 (100)	73	35.9 (82.3)	6.4
7.8% $WO_x/ZrPO_4$ [18]	56 (100)	22.5	0	0
MgO [9]	n/a	n/a	11	15
$Mg_{2.9}Al$ hydrotalcite [9]	n/a	n/a	74.3 (98)	162
1.2 wt% Li/CaO [11]	n/a	n/a	100	159.6
SO_4/ZrO_2	37 (94)	33	2.8 (13)	–
Nafion	20 (86)	12	1.6 (24)	–
HZSM-5	19 (81)	12	0 (10)	–

[a] After 3 h reaction, in parentheses after 24 h.

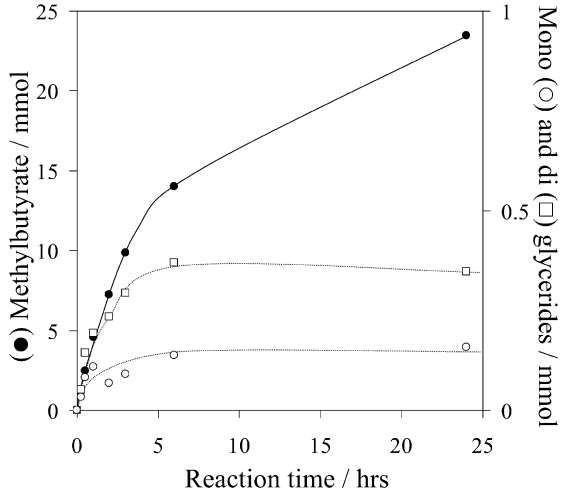

Fig. 9. Observed product distribution during $Cs_{2.3}H_{0.7}PW_{12}O_{40}$ catalyzed transesterification of tributyrin with methanol at 60 °C.

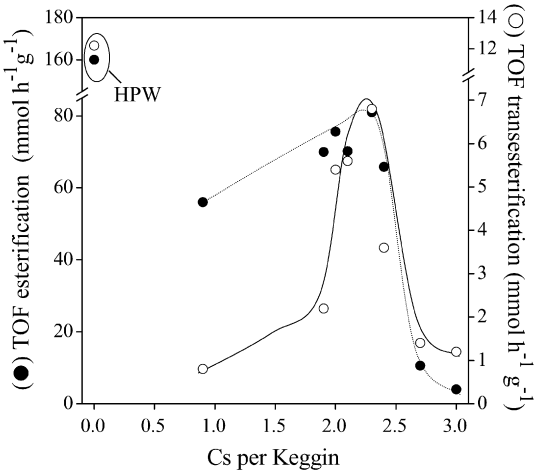

Fig. 10. Calculated TOF using Cs exchanged HPW catalysts in the esterification of palmitic acid and transesterification of tributyrin with methanol as a function of Cs content.

Fig. 10 compares the TOF of both reactions across the catalysts series. Note that whereas the parent HPW exhibits excellent activity for both transformations, it is, of course, completely soluble in these reaction media and thus unable to compete with the many process advantages offered by its heterogeneous counterparts. Low levels of Cs exchange confer comparatively poor activity in both palmitic acid esterification and tributyrin transesterification; however, further Cs incorporation promotes both reactions (especially transesterification) with the maximal TOF achieved for $Cs_{2.3}$ loadings. The best esterification rates of 81 mmol h^{-1} g^{-1} are far superior to that obtained for $ZrPO_4$-tethered phosophotungstic acid of 22.5 mmol h^{-1} g^{-1} [18], whereas the best transesterification rate of 6.4 mmol h^{-1} g^{-1} compares reasonably well with that for MgO at 15 mmol h^{-1} g^{-1}. Nonetheless, it should be noted that tailored solid bases, such as Li-doped CaO and MgAl hydrotalcites, can outperform the present solid acid system in tributyrin transesterification. Further Cs addition induces a dramatic drop in general catalytic activity, which we associate with the loss of Brönsted acid sites for stoichiometry approaching Cs_3 (apparent from both calorimetry data and α-pinene isomerization activity). The most active $Cs_{2.3}PW$ catalyst facilitated complete palmitic acid conversion in only 6 h (Table 4b). Further comparison of $Cs_{2.3}$ catalyst with other solid acid catalysts (Table 5) demonstrates that the $Cs_{2.3}$ sample outperforms SO_4/ZrO_2, Nafion, and H ZSM-5 in the esterification of palmitic acid. Likewise, all three commercial catalysts exhibit poor activity in the transesterification of tributyrin with methanol compared to $Cs_{2.3}$.

We performed leaching studies as detailed in Section 2 to determine whether soluble HPW components were released into the reaction. As predicted from our model, in which low-Cs loading samples are composed of Cs_3 particles capped by a pure HPW layer, the Cs_1 showed some dissolution of an active acid component after reflux in hot methanol. Indeed, powder XRD revealed the loss of HPW reflections from the surviving solid isolated after this methanol treatment of the Cs_1 salt. In contrast, materials with higher Cs content were stable to methanol reflux, confirming their heterogeneous mode of action.

Having demonstrated that the Cs-doped HPWs were separately active in both esterification and transesterification, we conducted a single-pot reaction with the $Cs_{2.3}$ catalyst to determine whether both palmitic acid esterification and tributyrin

Table 6
Conversion of tributyrin and palmitic acid after 6 h reaction during one-pot esterification and transesterification reactions using a fresh and recycled $Cs_{2.3}$ catalyst

Cycle	Conversion of tributyrin (%)	Conversion of palmitic acid (%)	Selectivity to methyl butyrate (%)	Selectivity to methyl palmitate (%)
1st	50.2	100.0	92.0	100
2nd	46.3	98.1	91.0	100
3rd	42.7	95.0	90.0	100

esterification could be undertaken simultaneously in a one-pot reaction, as is desirable for a commercial biodiesel process. Table 6 shows the conversions of both acid and triglyceride after the addition of 0.5 mmol palmitic acid to a transesterification reaction. We found 100% palmitic acid conversion along with 50.2% tributyrin conversion after 6 h of reaction, with 90% selectivity to the methyl ester achieved. In the absence of palmitic acid, tributyrin conversion was comparable, confirming the possibility of simultaneous esterification and transesterification without loss of activity or selectivity in the (secondary) transesterification process. The $Cs_{2.3}$ catalyst could be recycled at least three times, with only negligible loss of activity. Although the overall transesterification reaction is slower than that possible via a solid base-catalyzed reaction (Table 5), there are obvious process advantages to operating a single-bed reactor with one catalyst formulation, such as those offered by the present Cs-exchanged HPW solid acids.

4. Conclusion

Insoluble HPA salts of general formula $Cs_xH_{3-x}PW_{12}O_{40}$ ($x = 0.9$–3) have been investigated for solid acid esterification and transesterification reactions. Detailed surface and bulk characterization suggest these materials are composed of a Cs_3PW core with a capping HPW surface layer. XPS reveals two Cs environments, consistent with the surface-terminating layer of a cubic, closely packed Cs_3PW structure. NH_3 adsorption calorimetry, porosimetry, and α-pinene isomerization reveal that the total acid site density decreases with Cs ion exchange, with Cs loadings of $x = 2$–2.3 having the greatest number of accessible surface acid sites. Salts with this composition also showed optimum performance in palmitic acid esterification and tributyrin transesterification to methyl butyrate, consistent with the reaction occurring over the surface of the insoluble salts. All samples with $x > 1$ are resistant to leaching and can be recycled without major loss of activity. $Cs_{2.3}H_{0.7}PW_{12}O_{40}$ can be used in simultaneous esterification and transesterification reactions without loss of activity or selectivity.

Acknowledgments

K.N. thanks the Royal Society, London for the award of a Royal Society Indian Fellowship. K.W. gratefully acknowledges BP for financial support and the Royal Society for the award of an equipment grant.

References

[1] S.J. Clark, L. Wagner, M.D. Schrock, P.G. Pinnaar, J. Am. Oil Chem. Soc. 61 (1984) 1632.
[2] G. Huber, S. Iborra, A.V. Corma, Chem. Rev. 106 (2006) 4044.
[3] S. Romano, Vegetable Oils Fuels, in: Proc. Int. Conf. on Plant and Vegetable Oils as Fuels, ASAE, MI, USA, 1982, p. 106.
[4] F. Ma, M. Hanna, Bioresour. Technol. 70 (1999) 1.
[5] B. Freedman, E.H. Pryde, T.L. Mounts, J. Am. Oil Chem. Soc. 61 (1984) 1638.
[6] Y. Ono, T. Baba, Catal. Today 38 (1997) 321.
[7] E. Leclercq, A. Finiels, C. Moreau, J. Am. Oil Chem. Soc. 78 (2001) 1161.
[8] S. Gryglewicz, Bioresour. Technol. 70 (1999) 249.
[9] D.G. Cantrell, L.J. Gillie, A.F. Lee, K. Wilson, Appl. Catal. A Gen. 287 (2005) 183.
[10] M. Di Serio, M. Ledda, M. Cozzolino, G. Minutillo, R. Tesser, E. Santacesaria, Ind. Eng. Chem. Res. 45 (2006) 3009.
[11] R.S. Watkins, A.F. Lee, K. Wilson, Green Chem. 6 (2004) 335.
[12] D.E. López, J.G. Goodwin Jr., D.A. Bruce, E. Lotero, Appl. Catal. A Gen. 295 (2005) 97.
[13] M. Canakci, J.V. Gerpen, Trans. ASAE 42 (1999) 1203.
[14] A. Corma, H. Garcia, S. Iborra, J. Primo, J. Catal. 120 (1989) 78.
[15] F.S. Guner, A. Srikecioglu, S. Yilmaz, A.T. Erciyes, A. Erdem, J. Am. Oil Chem. Soc. 73 (1996) 347.
[16] M. Saroja, T.N.B. Kaimal, Synth. Commun. 16 (1986) 1423.
[17] K. Ramalinga, P. Vijayalakshmi, T.N.B. Kaimal, Tetrahedron Lett. 43 (2002) 879.
[18] K.N. Rao, A. Sridhar, A.F. Lee, S.J. Tavener, N.A. Young, K. Wilson, Green Chem. 8 (2006) 790.
[19] M. Di Serio, R. Tesser, M. Dimiccoli, F. Cammarota, M. Nasatasi, E. Santacesaria, J. Mol. Catal. A Chem. 239 (2005) 111.
[20] S. Furuta, H. Matsuhashi, K. Arata, Catal. Commun. 5 (2004) 721.
[21] N. Mizuno, M. Misono, Chem. Rev. 98 (1998) 199.
[22] T. Okuhara, N. Mizuno, M. Misono, Adv. Catal. 41 (1996) 113.
[23] M. Misono, Catal. Rev. Sci. Eng. 29 (1987) 269.
[24] A.D. Newman, D.R. Brown, P. Siril, A.F. Lee, K. Wilson, Phys. Chem. Chem. Phys. 8 (2006) 2893.
[25] T. Okuhara, T. Nishimura, H. Watanabe, M. Misono, J. Mol. Catal. 74 (1992) 247.
[26] T. Okuhara, T. Arai, T. Ichiki, K.Y. Lee, M. Misono, J. Mol. Catal. 55 (1989) 293.
[27] N. Mizuno, M. Misono, Chem. Lett. (1987) 967.
[28] T. Okuhara, T. Nakato, Catal. Surv. Jpn. 2 (1998) 31.
[29] P.F. Siril, D.R. Brown, J. Mol. Catal. A Chem. 252 (2006) 125.
[30] S.P. Felix, C.S. Jowitt, D.R. Brown, Thermochim. Acta 433 (2005) 59.
[31] N. Cardona Martinez, J.A. Dumesic, Adv. Catal. 38 (1992) 125.
[32] J.B. McMonagle, J.B. Moffat, J. Colloid Interface Sci. 101 (1985) 479.
[33] A. Corma, A. Martınez, C. Martınez, J. Catal. 164 (1996) 422.
[34] J.B. Highfield, B.K. Hodnett, J.B. McMonagle, J.B. Moffat, Proc. 8th Int. Congr. Catalysis, vol. 5, ed. IUPAC, Verlag Chemie, Frankfurt am Main, 1984, p. 611.
[35] K. Inumaru, T. Ito, M. Misono, Microporous Mesoporous Mater. 21 (1998) 629.
[36] G. Busca, Catal. Today 27 (1996) 323.
[37] J.A. Dias, E. Caliman, S. Claidia, L. Dias, Microporous Mesoporous Mater. 76 (2004) 221.
[38] T. Okuhara, H. Watanabe, T. Nishimura, K. Inamaru, M. Misono, Chem. Mater. 12 (2000) 2230.
[39] M. Misono, I. Ono, G. Koyano, A. Aoshima, Pure Appl. Chem. 72 (2000) 1305.